

IMPACT DAMAGE DETECTION ON SCARF-REPAIRED COMPOSITES USING LAMB WAVE SENSING

Ichiya Takahashi*, Yusaku Ito*, Shin-ichi Takeda**, Yutaka Iwahori**, Junji Takatsubo***, Nobuo Takeda*

*The University of Tokyo, **Japan Aerospace Exploration Agency, ***National Institute of Advanced Industrial Science and Technology

Keywords: CFRP, Scarf-repair, Adhesive debonding, Elastic-wave

Abstract

In this research, the health monitoring technique for the detection of impact damages on the scarf-repaired composites is established. We detect the debondings of adhesive layer by using the Lamb-waves propagating in the structures. We visualized Lamb waves propagating in scarf-repaired composites by pulsed-laser scanning and observed the change in the behavior of wave propagation due to the damages. We applied this technique to the scarf-repaired specimens with artificial defects. In these results, the reflection and scattering of the elastic waves at the boundary of defects were observed. These results indicate that this visualization technique is effective for the detection of impact damages in scarf-repaired composites.

1 Introduction

Carbon fiber reinforced plastics (CFRPs) have excellent mechanical properties such as high specific stiffness and specific strength. Therefore, they have been applied to airplane structures and have contributed to the weight reduction of such aircraft. More than 30 years have passed since composite materials were first introduced to civil aviation aircrafts. During this span of time, the weight percentage of composites to the whole weight of airplane has increased. Such drive will affect not only the design of aircrafts but also their maintenance. As the laminated composites are widely used in airframes, the number of repair cases on composite airframes will increase. Therefore, repair techniques are also required for laminated composites because the complete replacement of damaged parts with new parts is an expensive proposition. Scarf repairs as shown in Fig. 1 are one of the representatives of actual repair of composite airframes. Scarf-repaired parts will increase as

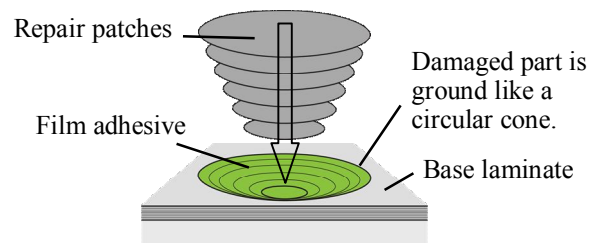


Fig. 1 Schematic of scarf repair on aircraft skin structures.

composites are widely used for the skins of aircrafts. When impact loadings are applied on the repaired part of composite airframes, they will bring critical damages on the whole structure. Thus, the health monitoring techniques to detect the impact damages in repaired composites need to be established.

Composite repairs have been studied by many researchers. For example, Ahn et al. evaluated the change in the tensile strength of scarf and step-lap joints after repair both experimentally and analytically [1][2]. Hu and Soutis calculated the compression strength of double-lap and scarf joints by FEM [3][4]. However, there are few researches about the evaluation of impact damages in repaired composites as far as we know. Smart composite patch systems in which health monitoring techniques were installed were also reported by several researchers [5-8]. In these researches, they detected the damages in the metallic structures repaired by composites due to the in-plane loadings such as static or fatigue loadings. In addition, they targeted the single/double sided patches as repairing methods. There are few researches about the impact damage detection in scarf-repaired composite structures as far as we know. In this research, health monitoring technique for the detection of impact damages in scarf-repaired composites is established. We detect the impact damages in scarf-repaired composites

with the change in the behavior of Lamb-wave propagation. First of all, we conducted the low-velocity impact test on the coupons imitating the adhesive part of scarf-repaired composites and observed impact damages. Secondly, elastic waves propagating in the scarf-repaired composites are visualized by use of a pulsed-laser scanning system. On the basis of the visualized results, we detect the impact damages in the scarf-repaired composites.

2 Low-velocity impact test of scarf-repaired composites

2.1 Manufacturing procedure of scarf-repaired specimen

The main material of specimens was laminated composites made of CFRP prepregs (IM600/#133, Toho Tenax Co., Ltd.). Epoxy film adhesive (FM1515-3M HT, Cytec Engineered Materials Inc.) was used for the bonding at the repair joint. The manufacturing procedure of specimen is shown in Fig. 2(a). CFRP composites were molded as the base laminates in advance. These laminates were ground at a certain taper angle in preparation for the base laminates. The taper angle is called "scarf angle". After that, prepregs were stacked as their edges shifted stepwise. These stacked laminates were called "repair laminates." Material and stacking sequence of the repair laminates are identical to those of base laminates. The film adhesive was attached on the surface of the tapered section in order to join the base laminate and the repair laminate. All the laminates were then molded using an autoclave. The curing temperature and time are 180 °C and 2 hours, respectively. Fig. 2(b) shows the cross-sectional micrograph of the specimen. The shape of step-like interface between the repair laminate and the adhesive layer is maintained after curing. The specimens used in this research can be seen as the combination of scarf joints and step-lap joints. As shown in Fig. 2(a), the cross-sectional geometry of the specimen corresponds to that of a half part of the actual scarf-repaired part. The stacking sequence of the specimens is $[+45/0/-45/90]_{2S}$. Scarf-angle was set to 2°.

2.2 Test procedure

For the low-velocity impact test, we drew upon the SRM 2R-94[9] in the SACMA (Suppliers of Advanced Composite Material Association) recommended method, which provides the evaluation method for compression after impact

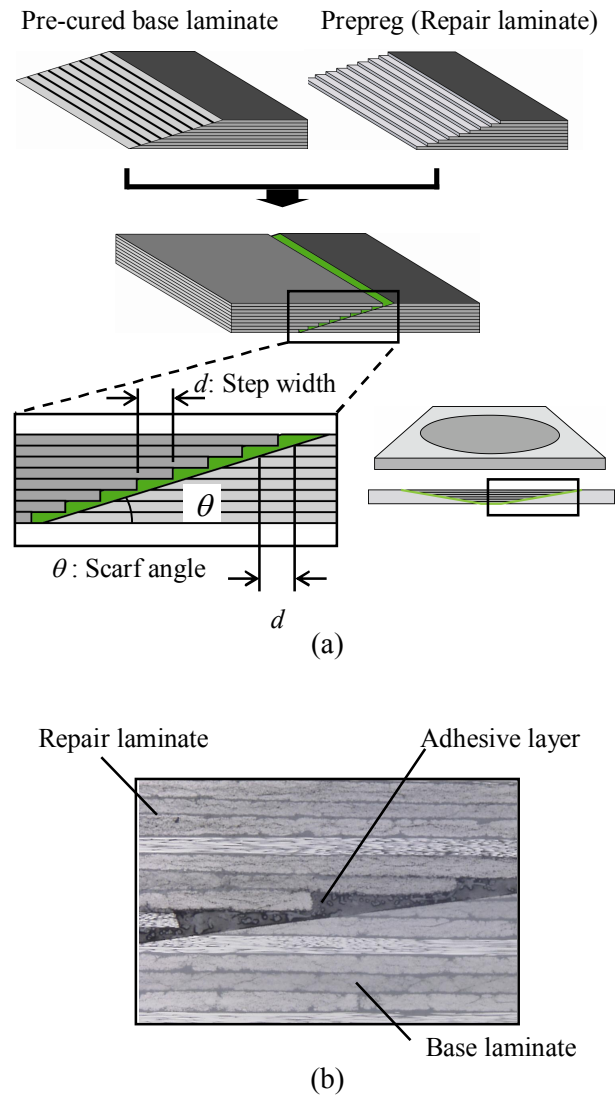


Fig. 2 (a) Schematic of the manufacturing procedure of the scarf joint specimen. (b) Cross-sectional micrograph of the specimen cross-section.

properties of oriented fiber resin composites. Fig. 3 shows the geometry and dimensions of the specimen used in the impact test. The dimensions of the specimens were set to 150 mm long and 100 mm wide according to the SRM 2R-94. Specimens were cut so that the center of adhesive part corresponds with that of specimen. An instrumented falling-weight impact machine (Dynatup 9250HV, Instron Corporation) was used for the impact tests. The diameter of the impactor is 15.8 mm. We prepared four specimens in the procedure mentioned in section 2.2. Impact load with different impact

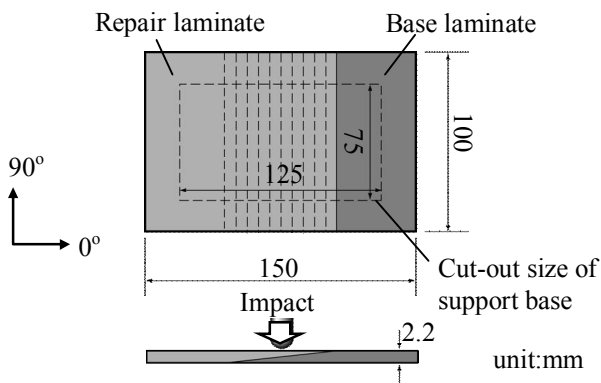


Fig. 3 Geometry and dimensions of the scarf-repaired specimen.

energy 2.0, 4.0, 6.0 and 8.0 J was applied on each specimen. The process of damage growth can be investigated by observing the change in damage configuration with the increase in impact energy. Ultrasonic inspections of the specimens were carried out before and after the impact tests. In addition, the cross-section around the impact point was also observed with a microscope after the impact tests.

2.3 Experimental results

Fig. 4(a) presents the ultrasonic inspection results. Impact damages were observed in all the results. Moreover, the damage area spread with the increase in applied impact energy. Fig. 4(b) shows the cross-sectional micrographs of the specimens. In the case of 2.0J, shear cracks and delaminations were observed near the impact point. These damages are typical impact damages in the CFRP laminates. In addition, the debonding at the interface between the adhesive layer and the repair laminate was observed on the upper side of the step-like adhesive interface. In the case of 4.0J, the debondings at the interface between the adhesive layer and the repair laminate were observed at two areas on the interface. Moreover, debonding on the lower side of the interface is found to be longer than that on the upper side. In the case of 6.0J, although the damage area in the C-Scan is about as large as that in the case of 4.0J, the debonding length became longer on the downside than that in the case of 4.0 J. In the case of 8.0J, the debonding of the adhesive layer reached the bottom surface. These results demonstrate that the debonding at the interface between the adhesive layer and the repair laminate arises from the shear cracks and delaminations near the impact point and propagates toward the bottom surface.

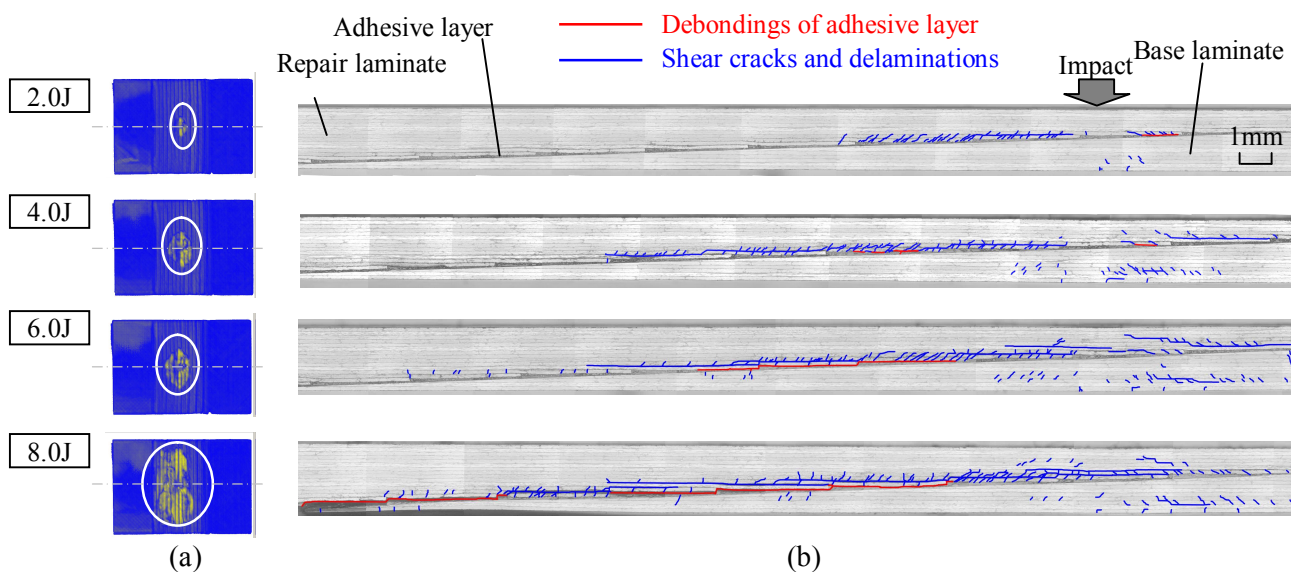


Fig. 4 Experimental results of the low-velocity impact test: (a) ultrasonic inspection results. (b) Micrographs of the central cross-section of specimens

3 Debonding detection using the change in the behavior of wave propagations

Debondings between adhesive layers and repair laminates in the scarf-repaired composites are considered as one of the most critical damages because they cause the reduction of stiffening effect and lead to the drop of whole repair patches during operations. Therefore, it is necessary to detect the adhesive debondings. In this research, we apply the wave-visualization technique using the pulsed-laser generating system to the detection of adhesive debondings in scarf-repaired composites. We manufactured scarf-repaired specimens with artificial defects imitating adhesive debondings and visualized the elastic waves propagating in the specimens.

3.1 Wave-visualization system

We used the wave-visualization system proposed by Takatsubo et al. [10]. A schematic of the wave-visualization system is illustrated in Fig. 5. Elastic waves are generated by illuminating a pulsed laser (YAG 1064nm, pulse duration 10nsec, beam diameter 2mm, and energy 5mJ) on the surface of specimen and received by a piezoelectric transducer attached on the surface. A pulsed-laser oscillator on a mechanical stage scans a given area on the surface. Waveforms at grid points in the scanned area are stored in a PC through an amplifier, a band-pass filter (BPF) and a digital oscilloscope. In this technique, it is not necessary to adjust the incident angle of the laser or focusing because pulsed-laser is used for the elastic-wave excitation. This technique is based on the assumption of "wave reversibility", which is mentioned in section 4. From this assumption, the time-history contour maps on the

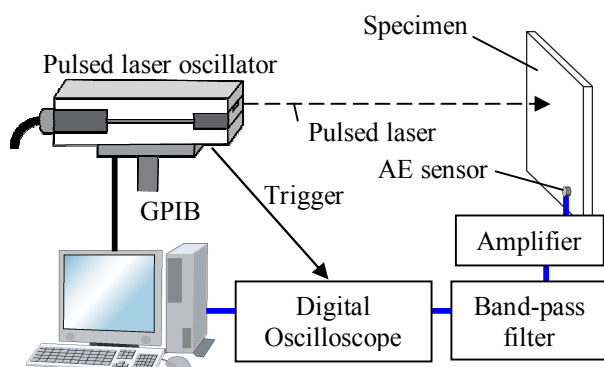


Fig. 5 Schematic of the measurement system for the visualization of the elastic-wave propagation.

wave amplitude at all grid points provide an image of elastic wave propagation in which as if they were oscillated at the fixed receiving point. When damages exist in the scanned area, scattering or reflection of elastic waves occur at the damage boundary, by which the damage can be detected.

3.2 Scarf repaired specimen with artificial defect

Materials and basic manufacturing procedure are the same as those mentioned in section 2.1. The stacking sequence of specimen is $[+45/0/-45/90]_{2S}$. Scarf-angle was set to 2° . Before attaching a film adhesive, we inserted a silicon rubber film (50 μm thick) between the repair laminate and the film adhesive as shown in Fig. 6 and pulled it out after curing. Fig. 6 (b) shows the cross-sectional micrograph of the specimen. Debonding was formed along the step-like interface between the repair laminate and adhesive layer. We manufactured two kinds of specimens with different-sized defects. Geometry and dimensions of the specimens and their defects are illustrated in Fig. 7 (a). Fig. 7 (b) shows the ultrasonic inspection of the specimens. Larger defect reached the bottom surface of the specimen. Adhesive part of the specimen was scanned with pulsed-laser oscillator. Scanning pitch was set to 0.5 mm x 0.5 mm.

3.3 Experimental results

Visualized results of the elastic waves propagating in the scarf-repaired specimen are presented in Fig. 8 ~ Fig. 10. We conducted three kinds of investigations in this experiment: influences of BPF, sensor position and damage size on the visualized results.

3.3.1 Influence of filtering

Fig. 8 (a) and (b) show the visualized results without filtering and that through a 200kHz BPF, respectively. Specimen used in this experiment is that with small defect. A transducer is attached on the top surface of the specimen as shown in Fig. 8. The value of t in each figure shows the time from when pulsed lasers were illuminated. As mentioned in section 3.1, elastic waves were visualized as if the waves had been generated at the received point. Moreover, the reflection and scattering of elastic waves were observed at the boundary of artificial debondings in both results. A variety of elastic waves with different velocities were observed in Fig. 8 (a). This is because the input wave generated by a

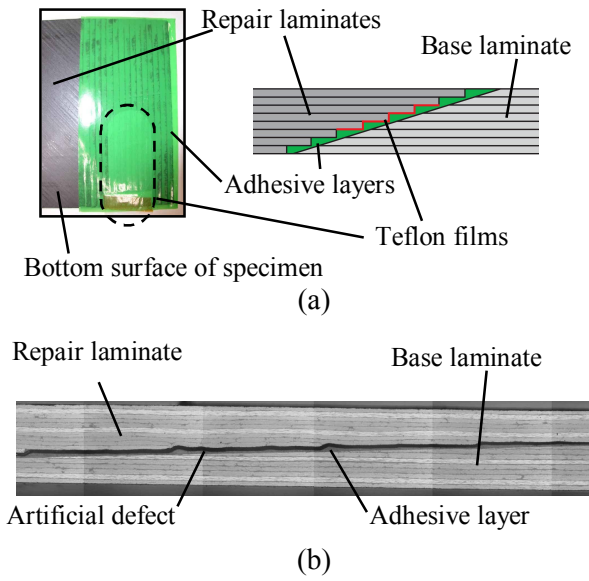


Fig. 6 (a) Manufacturing procedure of the specimen with artificial defect. (b) Micrograph of the cross-section of specimen.

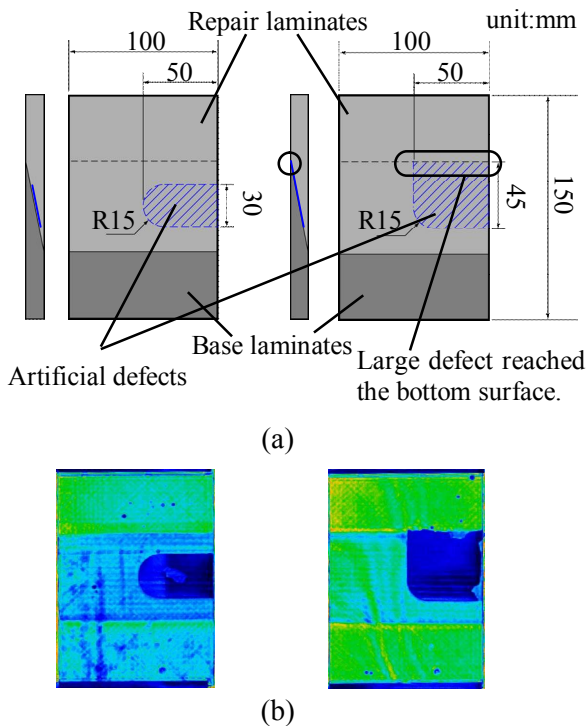


Fig. 7 (a) Geometry and dimensions of the specimens and artificial defects. (b) Ultrasonic inspection results of the specimen.

pulsed laser has a wide range of frequency components and the generated waves have dispersed when propagating in the specimen. In contrast, the result measured after filtering shows two kinds of

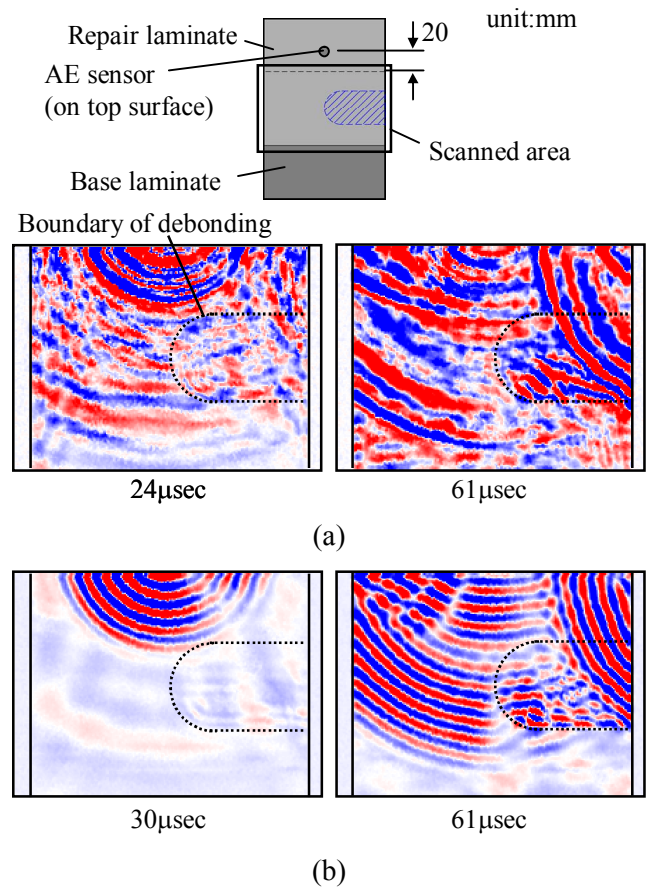


Fig. 8 Visualized results of elastic waves propagating in the scarf-repaired specimen. (a) without filtering. (b) through a 200kHz BPF.

waves with different velocities. The reflection and scattering of the faster wave was observed at 30 μsec. The slower wave, which has a larger amplitude than the faster one, reflected at the one-half of boundary more distant from the received point (lower side in the figure) at 61 μsec. Comparison of both results show that the shape of debonding was more difficult to detect in the result without filtering than that with filtering due to the existence of various kinds of waves, leading to the conclusion that the frequency components need to be selected by filtering the received wave signals before visualization.

3.3.2 Influence of sensor position

Fig. 9 (a) and (b) show the visualized results measured at two sensor positions. Fig. 9 (a) is identical to Fig. 8 (b). In the result of sensor B, almost no reflection and scattering of elastic waves were observed at the boundary of debonding. Instead, the stripe pattern like a concentric circle was skewed

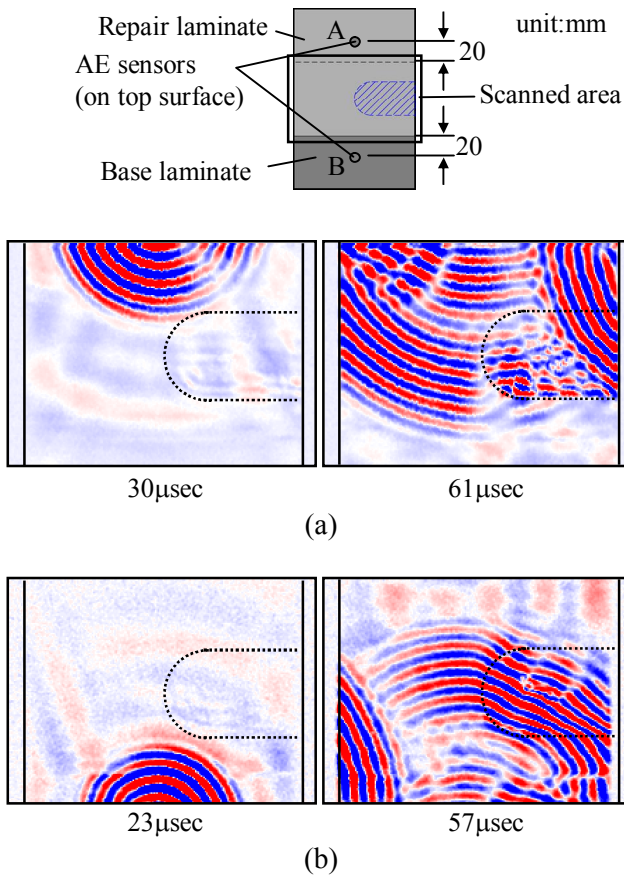


Fig. 9 Visualized results of elastic waves propagating in the scarf-repaired specimen: (a) sensor A and (b) sensor B.

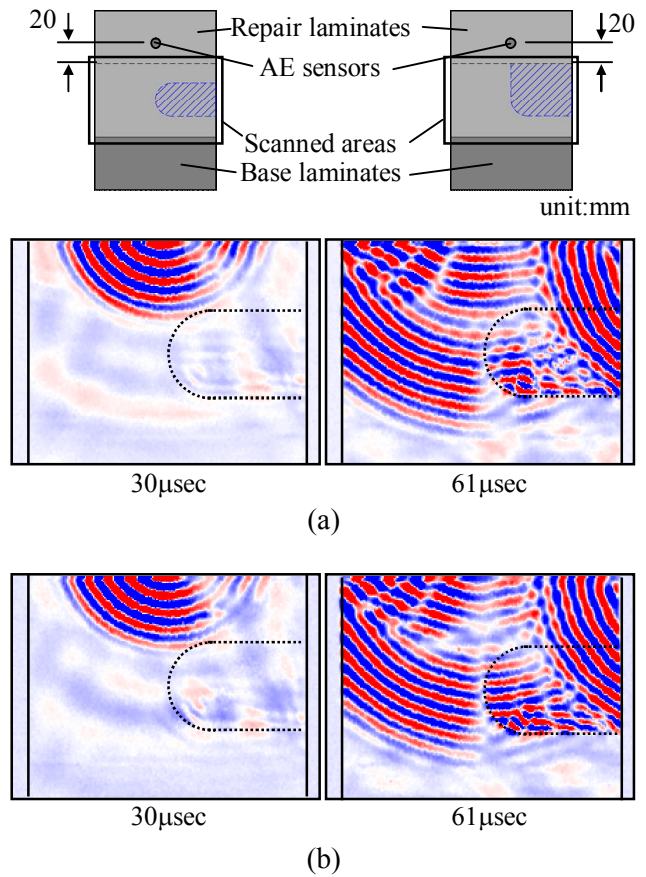


Fig. 10 Visualized results of elastic waves propagating in the scarf-repaired specimen: (a) small defect and (b) large defect.

at the boundary of debonding. Moreover, spacing between stripes lying on the debonding area became shorter than that out of the debonding. This is because the wave velocity decreases in the debonded region with the decrease of thickness.

3.3.3 Influence of damage size

Visualized results of the specimens with different-sized debondings are presented in Fig.10 (a) and (b). Two kinds of waves were observed in the results. They reflected and scattered at the one-half of boundary more distant from the received point, while almost no reflection and scattering were observed at the other half of boundary: there is the sensitivity difference in the debonding boundary. As a result, both visualized results are quite similar to each other, which means that it is difficult to identify the damage size in the structures on this test condition. Therefore, it is necessary to investigate the cause for the difference in sensitivity to damages.

There is a possibility that the difference in debonding depth from the top surface has an influence on the sensitivity. Debondings of adhesive layers occurs along the step-like interface, which brings the difference in the debonding depth. In our future works, the influence of debonding depth on the sensitivity is investigated.

4 Verification of wave reversibility

Visualization technique used in this research is based on the assumption of the reversibility of propagating waves: the waveform propagating between two points (A to B in Fig. 11) does not change even if the actuator and the sensor are exchanged (B to A). Takatsubo et al investigated the validity of this assumption in the case of aluminum plates and CFRP cross-ply laminates [10][11]. We experimentally investigated whether the assumption is valid even when this technique is applied to the scarf-repaired composites. Specimen used in this experiment is identical to that used in section 3 (with

smaller debonding). The positions of laser illumination and the transducer are illustrated in Fig. 12(a). Wave signal generated at point A by a pulsed laser was received at point B by a transducer, and stored without filtering. After that, we measured wave signals in the same procedure after exchanging the positions of laser illumination and the transducer. Fig. 12 (b) shows the comparison of two waveforms measured in this experiment. Although there is the difference in the amplitude at each time, waveforms are quite similar to each other. The main causes for the difference in amplitude of waveforms are (1) the difference in the configuration of wave-generating and receiving system such as the diameter of laser beam spot and that of the transducer and (2) the difference in the attachment condition of transducer and the position of two (generating and receiving) points between two measurements. Visualized image is characterized mainly by the relative difference in amplitude: positional relationship between the wave top and bottom. The amplitude value itself has little influence on the visualized images. Consequently, this result indicates that the assumption of wave reversibility is valid in the case of the application to scarf-repaired composites.

5 Conclusions

We conducted two kinds of experiments in order to establish impact damage detection system for the scarf-repaired composites: the low-velocity impact test and elastic-wave visualization test by use of a pulsed laser generating system. Impact test results demonstrate that the debonding at the interface between the adhesive layer and the repair laminate arises from the shear cracks and delaminations near the impact point and propagates toward the bottom surface. In the elastic-wave visualization test, the change in the behavior of wave propagation was observed at the boundary of debonding. Moreover, the detection sensitivity is found to vary between the parts of debonding boundary. These results indicate that this visualized technique is effective for the detection of the impact damages in scarf-repaired composites.

References

[1] Ahn S. H. and Springer G. S. "Repair of Composite Laminates-I: Test Results". Journal of Composite Materials, Vol. 32, No. 11, pp 1036-1074, 1998.

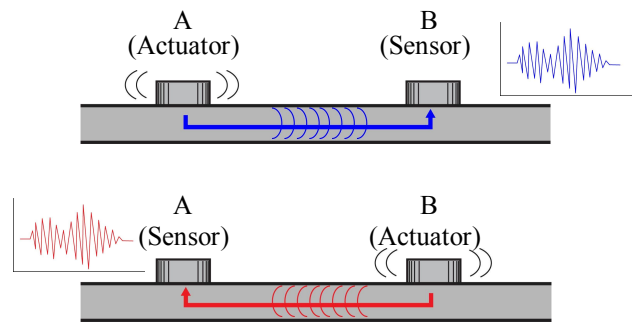


Fig. 11 Schematic of the reversibility of the ultrasonic waves.

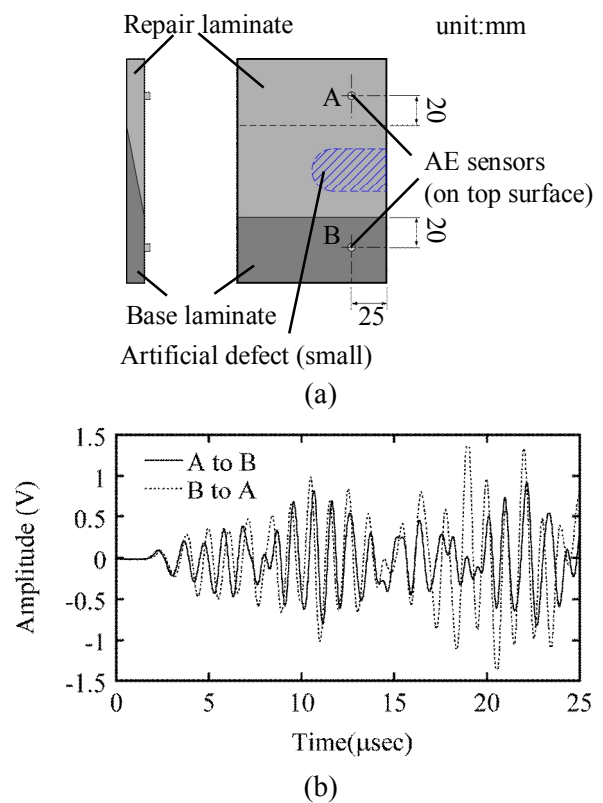


Fig. 12 (a) Position of the laser oscillation and the receiver for the verification of the wave reversibility. (b) Comparison of the waveforms between two propagation paths.

[2] Ahn S. H. and Springer G. S. "Repair of Composite Laminates-II: Models". Journal of Composite Materials, Vol. 32, No. 11, pp 1076-1114, 1998.

[3] Hu F. Z. and Soutis C. "Strength prediction of patch-repaired CFRP laminates loaded in compression". Composites Science and Technology, Vol. 60, pp 1103-1114, 1998.

- [4] Soutis C. and Hu F. Z. "Failure analysis of scarf-patch-repaired carbon fiber/epoxy laminates under compression". *AIAA Journal*, Vol. 38, No. 4, pp 737-740, 2000.
- [5] Ihn J. B. and Chang F. K. "Detection and monitoring of hidden fatigue crack growth using a built-in piezoelectric sensor/actuator network: I. Diagnostics". *Smart Materials and Structures*, Vol. 13, pp 609-620, 2004.
- [6] Ihn J. B. and Chang F. K. "Detection and monitoring of hidden fatigue crack growth using a built-in piezoelectric sensor/actuator network: II. Validation using riveted joints and repair patches". *Smart Materials and Structures*, Vol. 13, pp 621-630, 2004.
- [7] Jones R. and Galea S. "Health monitoring of composite repairs and joints using optical fibres". *Composite Structures*, Vol. 58, pp 397-403, 2002.
- [8] Koh Y. L., Rajic N., Chiu W. K. and Galea S. "Smart structure for composite repair". *Composite Structures*, Vol. 47, pp 745-752, 1999.
- [9] "SACMA recommended test method for compression after impact properties of oriented fiber-resin composites. SRM 2R-94". Suppliers of Advanced Composite Materials Association (SACMA), 1994.
- [10] Takatsubo J., Wang B., Tsuda H. and Toyama N. "Generation laser scanning method for the visualization of ultrasounds propagating on a 3-D object with an arbitrary shape (in Japanese)". *Transactions of the Japan Society of Mechanical Engineers, Series A*, Vol. 72, No. 718, pp 945-950, 2006.
- [11] Yashiro S., Takatsubo J., Toyama N., Okabe T. and Takeda N. "Delamination detection in holed CFRP laminates using visualized ultrasound propagation (in Japanese)". *Transactions of the Japan Society of Mechanical Engineers, Series A*, Vol. 72, No. 724, pp 1882-1887, 2006.

Acknowledgement

One of the authors I.T. was supported through the 21st Century COE Program, "Mechanical Systems Innovation," by the Ministry of Education, Culture, Sports, Science and Technology.